Event-Based Motion Segmentation by Motion Compensation

Timo Stoffregen[1,2], Guillermo Gallego[3], Tom Drummond[1,2], Lindsay Kleeman[1], Davide Scaramuzza[3]

[1]Dept. Electrical and Computer Systems Engineering, Monash University, Australia.
[2]Australian Centre of Excellence for Robotic Vision, Australia.
[3]Dept. Informatics (Univ. Zurich) and Dept. Neuroinformatics (Univ. Zurich & ETH Zurich), Switzerland.

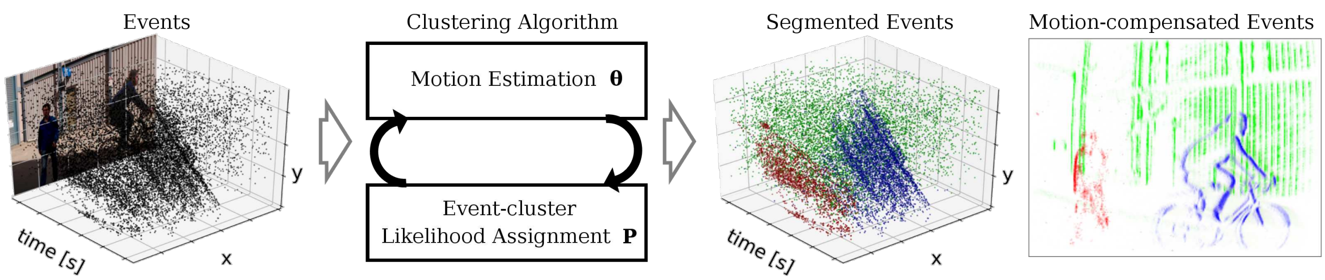

Figure 1: Our method segments a set of events produced by an event-based camera (Left, with color image of the scene for illustration) into the different moving objects causing them (Right: pedestrian, cyclist and camera's ego-motion, in color). We propose an iterative clustering algorithm (Middle block) that jointly estimates the motion parameters $\boldsymbol{\theta}$ and event-cluster membership probabilities $\mathbf{P}$ to best explain the scene, yielding motion-compensated event images on all clusters (Right).

Abstract

In contrast to traditional cameras, whose pixels have a common exposure time, event-based cameras are novel bio-inspired sensors whose pixels work independently and asynchronously *output intensity changes (called "events"), with microsecond resolution. Since events are caused by the apparent motion of objects, event-based cameras sample visual information based on the scene dynamics and are, therefore, a more natural fit than traditional cameras to acquire motion, especially at high speeds, where traditional cameras suffer from motion blur. However, distinguishing between events caused by different moving objects and by the camera's ego-motion is a challenging task. We present the first per-event segmentation method for splitting a scene into independently moving objects. Our method jointly estimates the event-object associations (i.e., segmentation) and the motion parameters of the objects (or the background) by maximization of an objective function, which builds upon recent results on event-based motion-compensation. We provide a thorough evaluation of our method on a public dataset, outperforming the state-of-the-art by as much as* $10\,\%$*. We also show the first quantitative evaluation of a segmentation algorithm for event cameras, yielding around* $90\,\%$ *accuracy at* 4 pixels *relative displacement.*

Supplementary Material

Accompanying video: https://youtu.be/0q6ap_OSBAk. We encourage the reader to view the added experiments and theory in the supplement.

1. Introduction

Event-based cameras, such as the Dynamic Vision Sensor (DVS) [1, 2], are novel, bio-inspired visual sensors. In contrast to conventional cameras that produce images at a fixed rate, the pixels in an event-based camera operate independently and asynchronously, responding to intensity changes by producing *events*. Events are represented by the x, y pixel location and timestamp t (in microseconds) of an intensity change as well as its polarity (i.e., whether the pixel became darker or brighter). Since event-based cameras essentially sample the scene at the same rate as the scene dynamics, they offer several advantages over conventional cameras: very high temporal resolution, low latency, very high dynamic range (HDR, $140\,\mathrm{dB}$) and low power and bandwidth requirements - traits which make them well suited to capturing motion. Hence, event-based cameras open the door to tackle challenging scenarios that are inaccessible to traditional cameras, such as high-speed and/or HDR tracking [3–6], control [7–9] and Simultaneous Localization and Mapping (SLAM) [10–13]. Due to their principle of operation and unconventional output, these cameras represent a paradigm shift in computer vision, and so, new algorithms are needed to unlock their capabilities. A survey paper on event-based cameras, algorithms, and applications, has been recently published in [2].

We consider the problem of segmenting a scene viewed by an event-based camera into independently-moving objects. In the context of traditional cameras, this problem is known as *motion segmentation* [14], and it is an essential pre-processing step for several applications in computer vision, such as surveillance, tracking, and recognition [15]. Its solution consists of analyzing two or more consecutive images from a video camera to infer the motion of objects and their occlusions. In spite of progress in this field, conventional cameras are not ideally suited to acquiring and analyzing motion; since exposure time is globally applied to all pixels, they suffer from motion blur in fast moving scenes. Event-based cameras are a better choice since they sample at exactly the rate of scene dynamics, but conventional techniques cannot be applied to the event data.

Motion segmentation in the case of a static event-based camera is simple, because in this scenario events are solely due to moving objects (assuming there are no changes in illumination) [16–18]. The challenges arise in the case of a moving camera, since in this scenario events are triggered everywhere on the image plane, produced by both the moving objects as well as the apparent motion of the static scene induced by the camera's ego-motion. Hence, event-based motion segmentation consists of classifying each event into a different object, including the background. However, each event carries very little information, and therefore it is challenging to perform the mentioned per-event classification.

We propose a method to tackle the event-based motion segmentation problem in its most general case, with a possibly moving camera. Inspired by classical layered models [19], our method classifies the events of a space-time window into separate clusters (i.e., "layers"), where each cluster represents a coherent moving object (or background) (see Fig. 1). The method jointly estimates the motion parameters of the clusters and the event-cluster associations (i.e., likelihood of an event belonging to a cluster) in an iterative, alternating fashion, using an objective function based on motion compensation [20, 21] (basically, the better the estimated unknowns, the sharper the motion-compensated event image of each cluster). Our method is flexible, allowing for different types of parametric motions of the objects and the scene (translation, rotation, zooming, etc.).

Contributions. In summary, our contributions are:

- A novel, iterative method for segmenting multiple objects based on their apparent motion on the image plane, producing a per-event classification into space-time clusters described by parametric motion models.
- The detection of independently moving objects without having to compute optical flow explicitly. Thus, we circumvent this difficult and error-prone step toward reaching the goal of motion-based segmentation.
- A thorough evaluation in challenging, real-world scenarios, such as high-speed and difficult illumination conditions, which are inaccessible to traditional cameras (due to severe motion blur and HDR), outperforming the state-of-the-art by as much as $10\,\%$, and showing that accuracy in resolving small motion differences between objects is a central property of our method.

As a by-product, our method produces sharp, motion-compensated images of warped events, which represent the appearance (i.e., shape or edge-map) of the segmented objects (or background) in the scene (Fig. 1, Right).

The rest of the paper is organized as follows: Section 2 reviews related work on event-based motion segmentation, Section 3 describes the proposed solution, which is then evaluated in Section 4. Conclusions are drawn in Section 5.

2. Related Work

Event-based motion segmentation in its non-trivial form (i.e., in the presence of event-clutter caused by camera ego-motion, or a scene with many independently moving, overlapping objects) has been addressed before [22–26].

In [22], a method is presented for detection and tracking of a circle in the presence of event clutter. It is based on the Hough transform using optical flow information extracted from temporal windows of events. Segmentation of a moving object in clutter was also addressed in [23]. It considered more generic object types than [22] by using event corners as primitives, and it adopted a learning technique to separate events caused by camera motion from those due to the object. However, the method required the additional knowledge of the robot joints controlling the camera.

Segmentation has been recently addressed by [24,25] using the idea of motion-compensated event images [20, 21, 27–30]. For example, [24] first fitted a motion compensation model to the dominant events, then removed these and fitted another motion model to the remaining events, greedily. Similarly, [25] detected moving objects in clutter by fitting a motion-compensation model to the dominant events (i.e., the background) and detecting inconsistencies with respect to that motion (i.e., the objects). The objects were then "segmented" via morphological operations on the warped image, and were used for tracking. The method could handle occlusions during tracking, but not during detection.

Our method differs from [22] in that we demonstrate segmentation on objects with arbitrary shapes, and from [23] in that we do not require additional inputs (e.g., robot joints). Our work is most related to [24, 25]; however, it has the following novelties: (*i*) it actually performs *per-event* segmentation, rather than just providing bounding boxes for detected object regions, (*ii*) it allows for general parametric motion models (as those in [20]) to describe each clus-

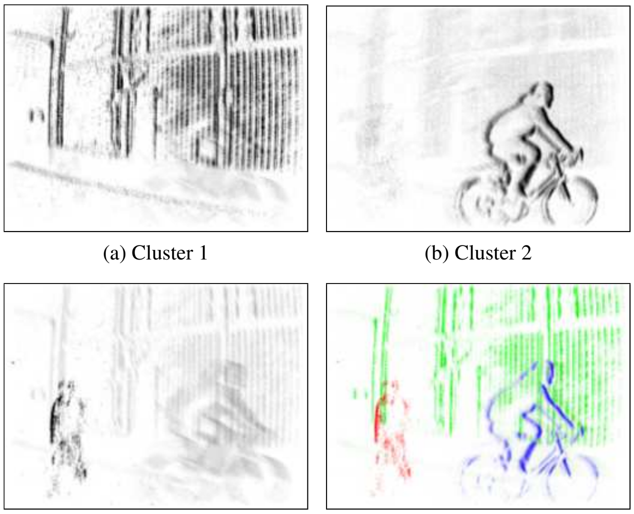

(a) Cluster 1 (b) Cluster 2

(c) Cluster 3 (d) All clusters (merged IWEs)

Figure 2: Our method splits the events into clusters (one per moving object), producing motion-compensated images of warped events (IWEs), as shown in (a)-(c) for the three objects in the scene of Fig. 1. The likelihood of each event is represented by the darkness of the pixel. Since the likelihoods are nonzero, "ghosts" can be seen in the individual clusters. IWEs in (a)-(c) are merged into a single image (d), using a different color for each cluster. Segmented events in upcoming experiments are shown using this colored motion-compensated image representation.

ter, (*iii*) it performs optimization based on a single objective function (as opposed to two sequential optimization criteria in [25]), (*iv*) it is able to handle occlusions between objects at any point in time. The proposed method, is, to our knowledge, the first one that *jointly* estimates the apparent motion parameters of all objects in the scene and the event-object associations (i.e., segmentation). It does so by leveraging the idea of motion-compensated event images within an iterative, alternating optimization approach, in an expectation-maximization (EM) fashion.

3. Methodology

Our method is inspired by the combination of classical layered models [19] and event-based motion compensation [20]. In the following, we review the working principle of event-based cameras, describe the motion segmentation problem addressed and present our proposed solution.

Event-Based Camera Working Principle. Event-based cameras, such as the DVS [1], have independent pixels that output "events" in response to intensity changes. Specifically, if $L(\mathbf{x},t) \doteq \log I(\mathbf{x},t)$ is the logarithmic intensity at pixel $\mathbf{x} \doteq (x,y)^\top$ on the image plane, the DVS generates an event $e_k \doteq (\mathbf{x}_k, t_k, s_k)$ if the change in intensity at pixel $\mathbf{x}_k$ reaches a threshold C (e.g., 10-15% relative change):

$$\Delta L(\mathbf{x}_k, t_k) \doteq L(\mathbf{x}_k, t_k) - L(\mathbf{x}_k, t_k - \Delta t_k) = s_k\, C, \quad (1)$$

where t_k is the timestamp of the event, Δt_k is the time since the previous event at the same pixel $\mathbf{x}_k$ and $s_k \in \{+1, -1\}$ is the polarity of the event (the sign of the intensity change).

3.1. Problem Statement

Since each event carries little information and we do not assume prior knowledge of the scene, we process events in packets (or groups) to aggregate sufficient information for estimation. Specifically, given a packet of events $\mathcal{E} \doteq \{e_k\}_{k=1}^{N_e}$ in a space-time volume of the image plane $V \doteq \Omega \times T$, we address the problem of classifying them into N_ℓ clusters (also called "layers"), with each cluster representing a coherent motion, of parameters $\boldsymbol{\theta}_j$. We assume that T is small enough so that the motion parameters of the clusters $\boldsymbol{\theta} \doteq \{\boldsymbol{\theta}_j\}_{j=1}^{N_\ell}$ are constant.

The images on both sides of the algorithm block in Fig. 1 illustrate the above-mentioned problem and its solution, respectively. Notice that, (i) since events have space-time coordinates, clusters are three-dimensional, contained in V, and (ii) since corresponding events (caused by the same point of a moving edge) describe point trajectories in V, optimal clusters should contain them, therefore, clusters have a "tubular" shape (Fig. 1, segmented events). Implicit in motion segmentation, if two objects share the same motion, they are segmented together, regardless of their location.

3.2. Summary of Proposed Solution

Leveraging the idea of motion compensation [20], we seek to separate the events $\mathcal{E}$ into clusters by maximizing *event alignment*, i.e., maximizing the sharpness of motion-compensated images (one per cluster) of warped events.

More specifically, the idea of motion compensation [20] is that, as an edge moves on the image plane, it triggers events on the pixels it traverses. The motion of the edge can be estimated by warping the events to a reference time and maximizing their alignment, producing a sharp Image of Warped Events (IWE) [20]. In the case of multiple objects with different motions, maximal event alignment cannot be achieved using a single warp, and so, several warps (i.e., motion models or "clusters") are required, as well as identifying which events belong to which object (i.e., "event-cluster associations"). This is the essence of our approach, which is illustrated in Figs. 1 and 2. Fig. 1 shows the events produced by three objects in a scene: a pedestrian, a cyclist and a the building facade (camera motion). Each object has a different motion and triggers events on the image plane as it moves. When events are warped to a reference time (e.g., $t_{\text{ref}} = 0$) according to a candidate motion model, they produce an IWE. If the candidate motion coincides with the true motion of the object causing the events, the warped events align, producing a sharp motion-compensated IWE, as shown in Fig. 2 using three different motion models (one per object). Otherwise, they do not align, producing a blurred IWE. We use the sharpness of such IWE as the main cue to segment the events. Our method jointly identifies the events corresponding to each independently moving object as well as the object's motion parameters.

3.3. Mathematical Formulation

In contrast to previous methods [24, 25], we explicitly model event-cluster associations in the motion-compensation framework, i.e., $p_{kj} = P(e_k \in \ell_j)$ is the probability of the k-th event belonging to the j-th cluster. Let $\mathbf{P} \equiv (p_{kj})$ be an $N_e \times N_\ell$ matrix with all event-cluster associations. The entries of $\mathbf{P}$ must be non-negative, and each row must add up to one. Using these associations, we define the *weighted* IWE of the j-th cluster as

$$I_j(\mathbf{x}) \doteq \textstyle\sum_{k=1}^{N_e} p_{kj}\, \delta(\mathbf{x} - \mathbf{x}'_{kj}), \tag{2}$$

with $\mathbf{x}'_{kj} = \mathbf{W}(\mathbf{x}_k, t_k; \boldsymbol{\theta}_j)$ the warped event location, and δ the Dirac delta. Equation (2) states that events are warped,

$$e_k \doteq (\mathbf{x}_k, t_k, s_k) \mapsto e'_k \doteq (\mathbf{x}'_k, t_{\text{ref}}, s_k), \tag{3}$$

and the values $p_{kj} \geq 0$ (i.e., weights) are accumulated at the warped locations $\mathbf{x}'_k$. Event alignment within the j-th cluster is measured using image contrast [31], which is defined by a sharpness/dispersion metric, such as the variance [20]:

$$\operatorname{Var}(I_j) \doteq \frac{1}{|\Omega|} \int_\Omega (I_j(\mathbf{x}) - \mu_{I_j})^2 d\mathbf{x}, \tag{4}$$

where μ_{I_j} is the mean of the IWE over the image plane Ω.

We propose to find the associations $\mathbf{P}$ and cluster parameters $\boldsymbol{\theta}$ that maximize the sum of contrasts of all clusters:

$$(\boldsymbol{\theta}^*, \mathbf{P}^*) = \underset{(\boldsymbol{\theta}, \mathbf{P})}{\arg\max} \sum_{j=1}^{N_\ell} \operatorname{Var}(I_j). \tag{5}$$

Since the problem addressed does not admit a closed-form solution, we devise an iterative, alternating optimization approach, which we describe in the next section.

The pseudo-code of our method is given in Algorithm 1. From the output of Algorithm 1, it is easy to compute motion-compensated images of events corresponding to each cluster, i.e., the weighted IWEs (2) shown in Fig. 2. Each IWE shows the sharp, recovered edge patterns (i.e, and appearance model) of the objects causing the events.

3.4. Alternating Optimization

Each iteration of Algorithm 1 has two steps (lines 6 and 7), as in a coordinate ascent algorithm. If the associations $\mathbf{P}$ are fixed, we may update the motion parameters

$$\boldsymbol{\theta} \leftarrow \boldsymbol{\theta} + \mu \nabla_{\boldsymbol{\theta}} \Big(\textstyle\sum_{j=1}^{N_\ell} \operatorname{Var}(I_j) \Big) \tag{6}$$

by taking a step ($\mu \geq 0$) in an ascent direction of the objective function (5) with respect to the motion parameters.

Algorithm 1 Event-based Motion Segmentation

```
1: Input: events E = {e_k}_{k=1}^{N_e} in a space-time volume V
   of the image plane, and number of clusters N_ℓ.
2: Output: cluster parameters θ = {θ_j}_{j=1}^{N_ℓ} and event-
   cluster assignments P ≡ p_kj ≐ P(e_k ∈ ℓ_j).
3: Procedure:
4: Initialize the unknowns (θ, P) (see Section 3.5).
5: Iterate until convergence:
6: • Compute the event-cluster assignments p_kj using (7).
7: • Update the motion parameters of all clusters (6).
```

Motion-compensation methods [20, 25] typically use gradient ascent or line search to solve for the motion parameters that maximize some objective function of the IWE. In our case, because the IWE (2) depends on both $\boldsymbol{\theta}$ and $\mathbf{P}$ and we seek to jointly estimate them, we do not wastefully search for the best $\boldsymbol{\theta}$ given the current estimate of $\mathbf{P}$. Instead, we update $\boldsymbol{\theta}$ using (6), proceed to refine $\mathbf{P}$ (see (7)), and iterate.

Fixing the motion parameters $\boldsymbol{\theta}$, we may refine the associations $\mathbf{P}$ using a closed-form probability partitioning law:

$$p_{kj} = \frac{c_j(\mathbf{x}'_k(\boldsymbol{\theta}_j))}{\sum_{i=1}^{N_\ell} c_i(\mathbf{x}'_k(\boldsymbol{\theta}_i))}, \tag{7}$$

where $c_j(\mathbf{x}) \neq 0$ is the local contrast (i.e., sharpness) of the j-th cluster at pixel $\mathbf{x}$, and it is given by the value of the weighted IWE, $c_j(\mathbf{x}) \doteq I_j(\mathbf{x})$. Thus, each event is softly assigned to each cluster based on how it contributes to the sharpness of all N_ℓ IWEs. The alternating optimization approach in Algorithm 1 resembles the EM algorithm, with the E-step given by (7) and the M-step given by (6).

3.5. Initialization

The proposed alternating method converges locally (i.e., there is no guarantee of convergence to a global solution), and it requires initialization of $\boldsymbol{\theta}, \mathbf{P}$ to start the iteration.

Several initialization schemes are possible, depending on the motion models. For example, if the warps of all clusters are of optical flow type, one could first extract optical flow from the events (e.g., using [32, 33]) and then cluster the optical flow vectors (e.g., using the k-means algorithm). The resulting cluster centers in velocity space would provide an initialization for the motion parameters of the clusters $\boldsymbol{\theta}$.

We follow a greedy approach, similar to that in [24], that works well in practice, providing cluster parameters close to the desired ones. It is valid regardless of the motion models used. We initialize events to have equal association probabilities, and then maximize the contrast of the first cluster with respect to its motion parameters. We then find the gradient of the local contrast for each event with respect to the motion parameters. Those events that belong to the cluster under consideration become less "in focus" when we move away from the optimized parameters, so those events that have a negative gradient are given a high association probability for that cluster and a low one for clusters subsequent. The process is repeated for the remaining clusters until all motion parameters $\boldsymbol{\theta}$ and associations $\mathbf{P}$ have been filled.

3.6. Discussion of the Segmentation Approach

The proposed approach is versatile, since it allows us to consider diverse parametric motion/warping models, such as linear motion (optic flow) [4, 20, 24], rotational motion [21], 4-DOF (degrees-of-freedom) motion [25], 8-DOF homographic motion [20], etc. Moreover, each cluster may have a different motion model, $\{\mathbf{W}_j\}_{j=1}^{N_\ell}$, as opposed to having a single model for all events, and therefore, all clusters. This characteristic is unique of our method.

It is also worth noting that the proposed method classifies events according to motion without having to explicitly compute optical flow, which is a widespread motion descriptor. Thus, our method is not simply optical flow clustering. Instead, our method encapsulates motion information in the warps of each cluster, thus by-passing the error-prone step of optical flow estimation in favor of achieving the desired goal of motion segmentation of the events.

The edge-like motion-compensated IWEs corresponding to each cluster are, upon convergence, a description of the intensity patterns (entangled with the motion) that caused the events. Thus our method recovers fine details of the appearance (e.g., shape) of the objects causing the events without having to estimate a (computationally expensive) 3D scene representation. In [25] fine details were only available for the dominant motion cluster.

Finally, the number of clusters N_ℓ is a hyper-parameter that may be tuned by a meta-algorithm (in the experiments, we set N_ℓ manually). This is a well-known topic in clustering [34]. While automatically determining the optimal N_ℓ depending on the scene is outside the scope of this paper, it should be noted that as we show in Section 4.3, our method is not sensitive to excess clusters N_ℓ.

3.7. Sequence Processing

The above method segments the events $\mathcal{E}$ from a short time interval T. To process an entire stream of events, a sliding window approach is used, splitting the stream into packets of events $\{\mathcal{E}_n\}_{n=1}^{N_g}$. We process the n-th packet and then slide the window, thus selecting more recent events. The motions estimated by clustering $\mathcal{E}_n$ can be propagated in time to predict an initialization for the clusters of the next packet, $\mathcal{E}_{n+1}$. We use a fixed number of events N_e per window, and slide by half of it, $N_e/2$.

4. Experiments

Overview. In this section we first provide a quantitative evaluation of our method on a publicly available, real-world dataset [25], showing that we significantly outperform two baseline methods [24, 25]. We provide further quantitative results on the accuracy of our method with regard to *relative motion differences* and we demonstrate the efficacy of our method on additional, challenging real-world data. Throughout the experiments, we demonstrate several features of our method, namely that (*i*) it allows arbitrary motion models for different clusters, (*ii*) it allows us to perform motion segmentation on difficult scenes (high speed and/or HDR), where conventional cameras would fail, (*iii*) it is robust to the number of clusters used (N_ℓ), and (*iv*) that it is able to perform motion segmentation on non-rigid scenes. The sequences considered cover a broad range of motion speeds, from $12\,\text{pixel/s}$ to several hundred pixel/s.

We strongly recommend looking at the accompanying video and supplementary material, where we present further experiments, including a comparison to "naive" k-means clustering, mixture density models and fuzzy-k-means.

The following experiments were carried out with data from a DAVIS240C camera [35], which provide both events and grayscale frames. The frames are not used in the experiments; they serve only an illustrative purpose.

4.1. Quantitative Evaluation

Results on Dataset from [25]. We ran our segmentation method on the Extreme Event Dataset (EED) from [25] and compared against the results from [25] and [24]. The sequences in the EED dataset showcase a range of scenes (Fig. 3 and Table 1) which are very challenging for conventional cameras. In particular, they comprise fast moving objects (around $600\,\text{pixel/s}$) in `Fast Moving Drone` and `Multiple Objects`, which are almost indiscernible on the frames provided by the DAVIS camera, as well as scenes with extreme lighting variations, such as `Lightning variation` (in which a drone is tracked despite a strobe light pointing at the camera), and object occlusions. Having object segmentation rather per-event segmentation in mind, the EED dataset provides timestamped bounding boxes around the moving objects in the scene and proposes to measure *object segmentation success* whenever the estimated bounding box overlaps at least $50\,\%$ with the hand-labeled one *and* it has more area within the hand-labeled bounding box than outside. To compare against [25], we perform motion segmentation on the events that occur around the timestamp of the bounding-box and count success if for a given cluster the above criterion is true for the segmented events. For a fair comparison, we used the same type of motion models (4-DOF warps) as in [25].

Table 1 reports the results of the comparison of our method against [24] and [25]. Our method outperforms [24] in all sequences by a large margin (from $7.41\,\%$ to $84.52\,\%$), and improves over [25] in all but one sequence, where it has comparable performance. In four out of five sequences we achieve accuracy above $92\,\%$, and in one of them, a

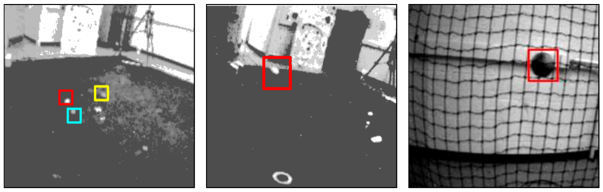

(a) (b) (c)

Figure 3: Several scenes from the Extreme Event Dataset (EED) [25]: (a) `Multiple Objects`, (b) `Occluded Sequence` and (c) `What is Background?` Moving objects (drones, balls, etc.) are within hand-labeled bounding boxes. Images have been brightened for visualization.

EED Sequence Name	SOFAS [24]	Mitrokhin [25]	Ours (Alg. 1)
`Fast moving drone`	88.89	92.78	**96.30**
`Multiple objects`	46.15	87.32	**96.77**
`Lighting variation`	0.00	**84.52**	80.51
`What is Background?`	22.08	89.21	**100.00**
`Occluded sequence`	80.00	90.83	**92.31**

Table 1: Comparison with state-of-the-art using the success rate proposed by [25] of detection of moving objects (in %).

perfect score, 100 %. Some results of the segmentation are displayed on the first columns of Fig. 4. In the `What is Background?` scene (1st column of Fig. 4), a ball is thrown from right to left behind a net while the camera is panning, following the ball. Our method clearly segments the scene into two clusters: the ball and the net, correctly handling occlusions. In the `Lightning variation` (2nd column of Fig. 4), a quadrotor flies through a poorly lit room with strobe lightning in the background, and our method is able to segment the events due to the camera motion (green and blue) and due to the quadrotor (purple).

Accuracy vs Displacement. While the dataset from [25] provides a benchmark for comparison against the state-of-the-art, it does not allow us to assess the *per-event* accuracy of our method. Here we measure segmentation success directly as a percentage of correctly classified events, thus much more fine-grained than with bounding boxes. Since real data contains a significant proportion of noise events, we perform the quantitative analysis on event data from a state-of-the-art photorealistic simulator [36]. Knowing which objects generated which events, allows us to finely resolve the accuracy of our method.

However, segmentation accuracy is closely coupled with the observation window over which events are collected. Intuitively, this makes sense; observing two objects with a relative velocity of 1 pixel/s for only 1 s means that the objects have moved only 0.1 pixels relative to each other, a difference that is difficult to measure. Observing these two objects for 10 s means a relative displacement of 10 pixels, which is easier to distinguish.

Fig 5 evaluates the above effect on a sequence consisting of textured pebbles moving with different relative velocities (Fig. 5a, with events colored in red and blue, according to polarity). The plot on Fig 5b shows that as the relative displacement increases, the proportion of correctly classified events, and therefore, the segmentation accuracy, increases. Our method requires that roughly 4 pixels of relative displacement have occurred in order to achieve 90 % accuracy. This holds true for any relative velocity.

Computational Performance. The complexity of Algorithm 1 is linear in the number of clusters, events, pixels of the IWE and the number of optimization iterations, in total, $O((N_e + N_p)N_\ell N_{\text{it}})$. Our method generally converges in less than ten iterations of the algorithm, although this clearly depends on several parameters, such as the data processed. Further details are given in the supplementary material. Here, we provide a ballpark figure for the processing speed. We ran our method on a single core, 2.4 GHz CPU where we got a throughput of 240 000 events/s for optical-flow–type warps (Table 2). Almost 99 % of the time was spent in warping events, which is parallelizable. Using a GeForce 1080 GPU, we achieved a 10× speed-up factor, as reported in Table 2. The bottleneck is not in computation but rather in memory transfer to and from the GPU.

Throughput decreases as N_ℓ increases, since all of the events need to be warped for every extra cluster in order to generate motion compensated images. Further, extra clusters add to the dimensionality of the optimization problem that is solved during the motion-compensation step.

N_ℓ	CPU [kevents/s]	GPU [kevents/s]
2	239.86	3963.20
5	178.19	1434.66
10	80.93	645.02
20	32.43	331.50
50	12.62	113.78

Table 2: Throughput in kilo-events per second (optical-flow type [24]) of Algorithm 1 running on a single CPU core vs GPU for varying N_ℓ (using the test sequence in Fig. 7).

Regardless of throughput, our method allows exploiting key features of event cameras, such as its very high temporal resolution and its HDR, as shown in experiments on the EED dataset (Table 1) and on some sequences in Fig. 4 (Vehicle facing the sun, Fan and coin).

4.2. Further Real-World Sequences

We test our method on additional sequences in a variety of real-world scenes, as shown in Fig. 4. The third column shows the results of segmenting a traffic scene, with the camera placed parallel to a street and tilting upwards while vehicles pass by in front of it. The algorithm segmented the

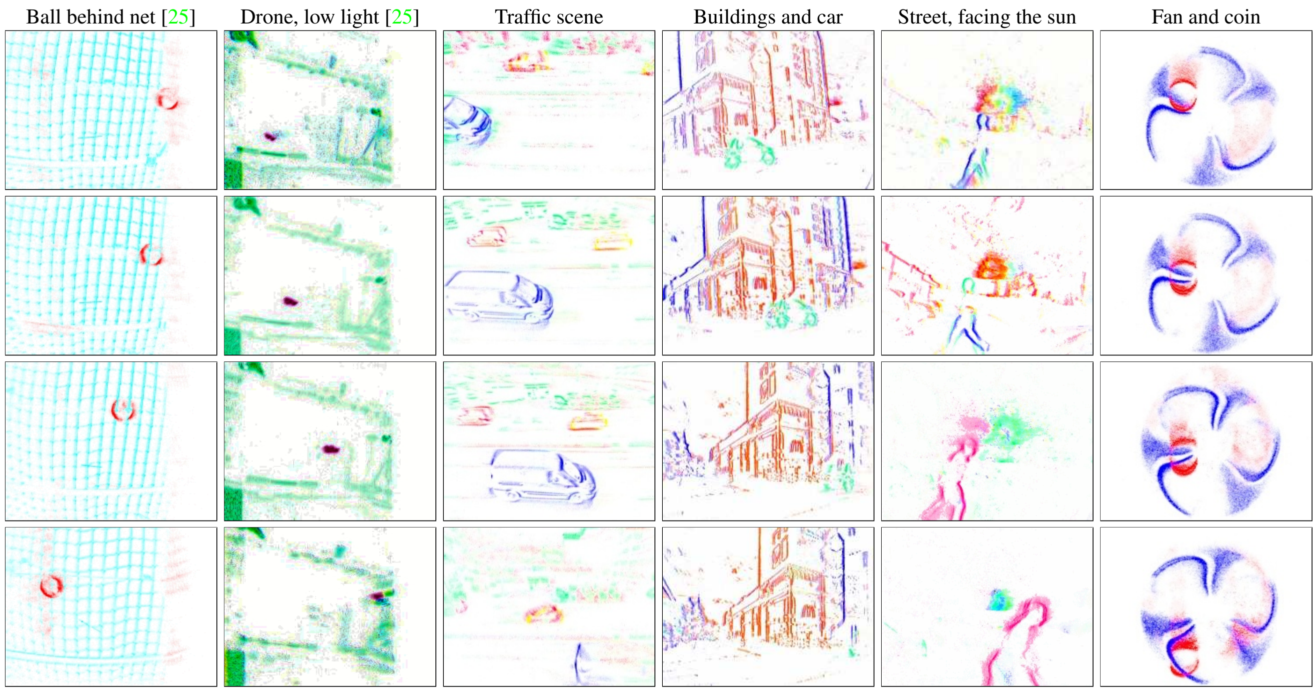

Figure 4: From top to bottom: snapshots (motion-compensated images, as in Fig.2) of events segmented into clusters on multiple sequences (one per column). Events colored by cluster membership. Best viewed in the accompanying video.

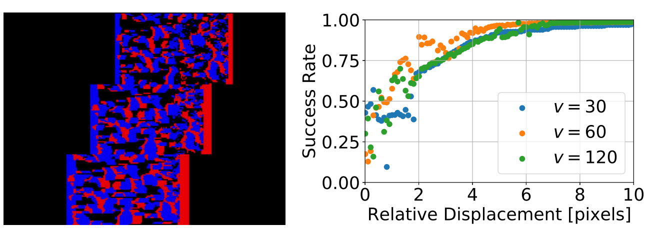

(a) Events (red and blue).

(b) Success Rate.

Figure 5: *Per-event Success Evaluation.* Segmentation accuracy vs relative object displacement (5b) on `pebbles` sequence (5a) at various relative velocities of objects $v_{\text{rel}} = \{30, 60, 120\}\text{pixel/s}$).

scene into four clusters: three corresponding to the vehicles (blue, red, yellow) and another one corresponding to the background buildings (ego-motion, in green). Even the cars going in the same direction are separated (red and yellow), since they travel at different speeds.

The fourth column of Fig. 4 shows the results of segmenting a scene with a car and some buildings while the camera is panning. We ran the algorithm to segment the scene into three clusters using optical flow warps. One cluster segments the car, and the other two clusters are assigned to the buildings. Note that the algorithm detects the differences in optical flow due to the perspective projection of the panning camera: it separates the higher speed in the periphery (blue) from the slower speed in the image center (red).

An HDR scene is shown on the fifth column of Fig. 4. The camera is mounted on a moving vehicle facing the sun (central in field of view) while a pedestrian and a skateboarder cross in front of it. The camera's forward motion causes fewer events from the background than in previous (panning) examples. We run the segmentation algorithm with six clusters, allowing the method to adapt to the scene. Segmented events are colored according to cluster membership. The algorithm correctly segments the pedestrian and the skateboarder, producing motion-compensated images of their silhouettes despite being non-rigidly moving objects.

Finally, the last column of Fig. 4 shows the versatility of our method to accommodate different motion models for each cluster. To this end, we recorded a coin dropping in front of the blades of a ventilator spinning at $1800\,\text{rpm}$. In this case the fan is represented by a rotational motion model and the coin by a linear velocity motion model. Our method converges to the expected, optimal solution, as can be seen in the motion compensated images, and it can handle the occlusions on the blades caused by the coin.

Fig. 6 shows that our method also works with a higher resolution (640×480 pixels) event-based camera [37]. More experiments are provided in the Appendix.

4.3. Sensitivity to the Number of Clusters

The following experiment shows that our method is not sensitive to the number of clusters chosen N_ℓ. We found that N_ℓ is not a particularly important parameter; if it cho-

(a) Scene (b) Segmentation into clusters

Figure 6: A 640×480 pixel DVS [37] panning over a slanted plane. Segmentation with 10 optical flow clusters (colored).

sen to be too large, the unnecessary clusters end up not having any events allocated to them and thus "die". This is a nice feature, since it means that in practice N_ℓ can simply be chosen to be large and then not be worried about. We demonstrate this on the `slider_depth` sequence from [38]; where there are multiple objects at different depths (depth continuum), with the camera sliding past them. Because of parallax, this results in a continuum of image plane velocities and thus infinitely many clusters would in theory be needed to segment the scene with an optical flow motion-model. Thus the sequence can only be resolved by adding many clusters which discretize the continuum of velocities.

Fig. 7 demonstrates that our method is robust with regard to the number of clusters chosen (in Figs. 7b–7d); too few clusters and the method will simply discretize the event cluster continuum, too many clusters and some clusters will "collapse", i.e., no events will be assigned to them. By segmenting with enough clusters and preventing cluster collapse, our method can be used to detect depth variations; nevertheless, tailored methods for depth estimation [39] are more suitable for such a task. The experiment also shows that our method deals with object occlusions.

Similarly, Fig. 7 shows that our method is not sensitive to the mixture of motion models either. Fig. 7e shows the result with five clusters of optical flow type and five clusters of rotation type. As can be seen, our method essentially allocates no event likelihoods to these rotation models clusters, which clearly do not suit any of the events in this sequence. Fig. 7f shows the result of using only rotation motion models, resulting in failure, as expected. As future work, a meta-algorithm could be used to select which motion models are most relevant depending on the scene.

5. Conclusion

In this work we presented the first method for per-event segmentation of a scene into multiple objects based on their apparent motion on the image plane. We jointly segmented a given set of events and recovered the motion parameters of the different objects (clusters) causing them. Additionally, as a by-product, our method produced motion-compensated images with the sharp edge-like appearance of the objects in the scene, which may be used for further analysis (e.g., recognition). We showed that our method outperforms two recent methods on a publicly available dataset (with as much as 10 % improvement over the state-of-the-art [25]), and showed it can resolve small relative motion differences between clusters. Our method achieves this using a versatile cluster model and avoiding explicit estimation of optical flow for motion segmentation, which is error prone. All this allowed us to perform motion segmentation on challenging scenes, such as high speed and/or HDR, unlocking the outstanding properties of event-based cameras.

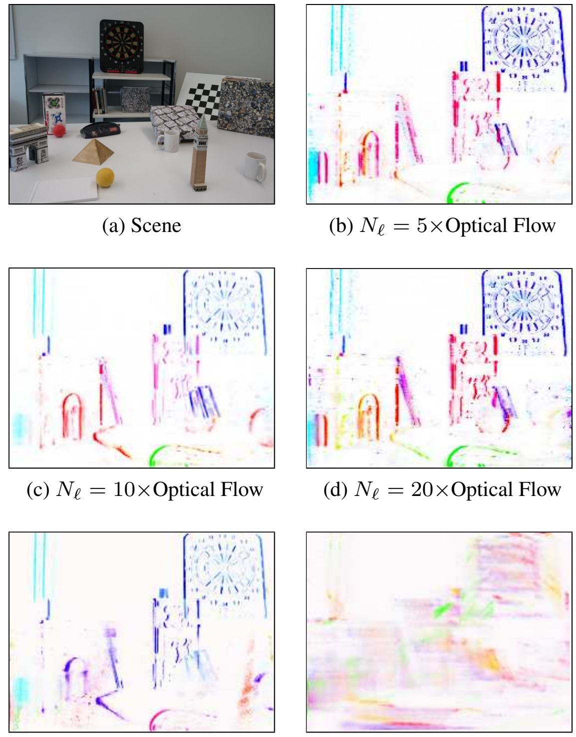

(a) Scene (b) $N_\ell = 5\times$Optical Flow

(c) $N_\ell = 10\times$Optical Flow (d) $N_\ell = 20\times$Optical Flow

(e) $N_\ell = 5\times\mathrm{OF}+5\times$Rotation (f) $N_\ell = 10\times$Rotation

Figure 7: *Experiment on* `slider_depth` *sequence* of [38]. Motion-compensated images in 7b to 7f show events colored by cluster. Using optical flow (OF) warps (in 7b–7d), event clusters correspond to depth planes with respect to the camera. Using as few as five clusters, the events are discretized and approximately spread over the depth continuum. Using 5, 10 or 20 clusters in 7b, 7c, 7d gives very similar results, showing that our method is fairly insensitive to the value of N_ℓ chosen. Adding clusters with motion models that do not suit the motion, as in 7e, where five clusters are pure rotational warps, does not much disturb the output either.

Acknowledgments. This work was supported by the Swiss National Center of Competence in Research Robotics, through the Swiss National Science Foundation and the SNSF-ERC Starting Grant as well as the ARC Centre of Excellence for Robot Vision, project #CE140100016.

References

[1] Patrick Lichtsteiner, Christoph Posch, and Tobi Delbruck, "A 128×128 120 dB 15 μs latency asynchronous temporal contrast vision sensor," *IEEE J. Solid-State Circuits*, vol. 43, no. 2, pp. 566–576, 2008. 1, 3

[2] Guillermo Gallego, Tobi Delbruck, Garrick Orchard, Chiara Bartolozzi, Brian Taba, Andrea Censi, Stefan Leutenegger, Andrew Davison, Jörg Conradt, Kostas Daniilidis, and Davide Scaramuzza, "Event-based vision: A survey," *arXiv:1904.08405*, 2019. 1, 2

[3] Elias Mueggler, Basil Huber, and Davide Scaramuzza, "Event-based, 6-DOF pose tracking for high-speed maneuvers," in *IEEE/RSJ Int. Conf. Intell. Robot. Syst. (IROS)*, pp. 2761–2768, 2014. 1

[4] Alex Zihao Zhu, Nikolay Atanasov, and Kostas Daniilidis, "Event-based feature tracking with probabilistic data association," in *IEEE Int. Conf. Robot. Autom. (ICRA)*, pp. 4465–4470, 2017. 1, 5

[5] Guillermo Gallego, Jon E. A. Lund, Elias Mueggler, Henri Rebecq, Tobi Delbruck, and Davide Scaramuzza, "Event-based, 6-DOF camera tracking from photometric depth maps," *IEEE Trans. Pattern Anal. Mach. Intell.*, vol. 40, pp. 2402–2412, Oct. 2018. 1

[6] Daniel Gehrig, Henri Rebecq, Guillermo Gallego, and Davide Scaramuzza, "EKLT: Asynchronous photometric feature tracking using events and frames," *Int. J. Comput. Vis.*, 2019. 1

[7] Jörg Conradt, Matthew Cook, Raphael Berner, Patrick Lichtsteiner, Rodney J. Douglas, and Tobi Delbruck, "A pencil balancing robot using a pair of AER dynamic vision sensors," in *IEEE Int. Symp. Circuits Syst. (ISCAS)*, pp. 781–784, 2009. 1

[8] Tobi Delbruck and Manuel Lang, "Robotic goalie with 3ms reaction time at 4% CPU load using event-based dynamic vision sensor," *Front. Neurosci.*, vol. 7, p. 223, 2013. 1

[9] Erich Mueller, Andrea Censi, and Emilio Frazzoli, "Low-latency heading feedback control with neuromorphic vision sensors using efficient approximated incremental inference," in *IEEE Conf. Decision Control (CDC)*, 2015. 1

[10] Hanme Kim, Stefan Leutenegger, and Andrew J. Davison, "Real-time 3D reconstruction and 6-DoF tracking with an event camera," in *Eur. Conf. Comput. Vis. (ECCV)*, pp. 349–364, 2016. 1

[11] Henri Rebecq, Timo Horstschäfer, Guillermo Gallego, and Davide Scaramuzza, "EVO: A geometric approach to event-based 6-DOF parallel tracking and mapping in real-time," *IEEE Robot. Autom. Lett.*, vol. 2, no. 2, pp. 593–600, 2017. 1

[12] Alex Zihao Zhu, Nikolay Atanasov, and Kostas Daniilidis, "Event-based visual inertial odometry," in *IEEE Conf. Comput. Vis. Pattern Recog. (CVPR)*, pp. 5816–5824, 2017. 1

[13] Antoni Rosinol Vidal, Henri Rebecq, Timo Horstschaefer, and Davide Scaramuzza, "Ultimate SLAM? combining events, images, and IMU for robust visual SLAM in HDR and high speed scenarios," *IEEE Robot. Autom. Lett.*, vol. 3, pp. 994–1001, Apr. 2018. 1

[14] Luca Zappella, Xavier Lladó, and Joaquim Salvi, "Motion segmentation: A review," in *Conf. Artificial Intell. Research and Development*, pp. 398–407, 2008. 2

[15] Björn Ommer, Theodor Mader, and Joachim M. Buhmann, "Seeing the objects behind the dots: Recognition in videos from a moving camera," *Int. J. Comput. Vis.*, vol. 83, pp. 57–71, Feb. 2009. 2

[16] Martin Litzenberger, Christoph Posch, D. Bauer, Ahmed Nabil Belbachir, P. Schön, B. Kohn, and H. Garn, "Embedded vision system for real-time object tracking using an asynchronous transient vision sensor," in *Digital Signal Processing Workshop*, pp. 173–178, 2006. 2

[17] Zhenjiang Ni, Sio-Hoï Ieng, Christoph Posch, Stéphane Régnier, and Ryad Benosman, "Visual tracking using neuromorphic asynchronous event-based cameras," *Neural Computation*, vol. 27, no. 4, pp. 925–953, 2015. 2

[18] Ewa Piatkowska, Ahmed Nabil Belbachir, Stephan Schraml, and Margrit Gelautz, "Spatiotemporal multiple persons tracking using dynamic vision sensor," in *IEEE Conf. Comput. Vis. Pattern Recog. Workshops (CVPRW)*, pp. 35–40, 2012. 2

[19] John YA Wang and Edward H Adelson, "Layered representation for motion analysis," in *IEEE Conf. Comput. Vis. Pattern Recog. (CVPR)*, pp. 361–366, 1993. 2, 3

[20] Guillermo Gallego, Henri Rebecq, and Davide Scaramuzza, "A unifying contrast maximization framework for event cameras, with applications to motion, depth, and optical flow estimation," in *IEEE Conf. Comput. Vis. Pattern Recog. (CVPR)*, pp. 3867–3876, 2018. 2, 3, 4, 5

[21] Guillermo Gallego and Davide Scaramuzza, "Accurate angular velocity estimation with an event camera," *IEEE Robot. Autom. Lett.*, vol. 2, no. 2, pp. 632–639, 2017. 2, 5

[22] Arren Glover and Chiara Bartolozzi, "Event-driven ball detection and gaze fixation in clutter," in *IEEE/RSJ Int. Conf. Intell. Robot. Syst. (IROS)*, pp. 2203–2208, 2016. 2

[23] Valentina Vasco, Arren Glover, Elias Mueggler, Davide Scaramuzza, Lorenzo Natale, and Chiara Bartolozzi, "Independent motion detection with event-driven cameras," in *IEEE Int. Conf. Adv. Robot. (ICAR)*, 2017. 2

[24] Timo Stoffregen and Lindsay Kleeman, "Simultaneous optical flow and segmentation (SOFAS) using Dynamic Vision Sensor," in *Australasian Conf. Robot. Autom. (ACRA)*, 2017. 2, 4, 5, 6

[25] Anton Mitrokhin, Cornelia Fermuller, Chethan Parameshwara, and Yiannis Aloimonos, "Event-based moving object detection and tracking," in *IEEE/RSJ Int. Conf. Intell. Robot. Syst. (IROS)*, 2018. 2, 3, 4, 5, 6, 7, 8

[26] Francisco Barranco, Ching L. Teo, Cornelia Fermuller, and Yiannis Aloimonos, "Contour detection and characterization for asynchronous event sensors," in *Int. Conf. Comput. Vis. (ICCV)*, 2015. 2

[27] Guillermo Gallego, Mathias Gehrig, and Davide Scaramuzza, "Focus is all you need: Loss functions for event-based vision," in *IEEE Conf. Comput. Vis. Pattern Recog. (CVPR)*, pp. 12280–12289, 2019. 2

[28] Timo Stoffregen and Lindsay Kleeman, "Event cameras, contrast maximization and reward functions: An analysis," in *IEEE Conf. Comput. Vis. Pattern Recog. (CVPR)*, pp. 12300–12308, 2019. 2

[29] Alex Zihao Zhu, Liangzhe Yuan, Kenneth Chaney, and Kostas Daniilidis, "Unsupervised event-based learning of optical flow, depth, and egomotion," in *IEEE Conf. Comput. Vis. Pattern Recog. (CVPR)*, 2019. 2

[30] Laurent Dardelet, Sio-Hoi Ieng, and Ryad Benosman, "Event-based features selection and tracking from intertwined estimation of velocity and generative contours," *arXiv:1811.07839*, 2018. 2

[31] Rafael C. Gonzalez and Richard Eugene Woods, *Digital Image Processing*. Pearson Education, 2009. 4

[32] Ryad Benosman, Charles Clercq, Xavier Lagorce, Sio-Hoi Ieng, and Chiara Bartolozzi, "Event-based visual flow," *IEEE Trans. Neural Netw. Learn. Syst.*, vol. 25, no. 2, pp. 407–417, 2014. 4

[33] Alex Zihao Zhu, Liangzhe Yuan, Kenneth Chaney, and Kostas Daniilidis, "EV-FlowNet: Self-supervised optical flow estimation for event-based cameras," in *Robotics: Science and Systems (RSS)*, 2018. 4

[34] C. Fraley, "How many clusters? Which clustering method? Answers via model-based cluster analysis," *The Computer Journal*, vol. 41, pp. 578–588, Aug. 1998. 5

[35] Christian Brandli, Raphael Berner, Minhao Yang, Shih-Chii Liu, and Tobi Delbruck, "A 240x180 130dB 3us latency global shutter spatiotemporal vision sensor," *IEEE J. Solid-State Circuits*, vol. 49, no. 10, pp. 2333–2341, 2014. 5

[36] Henri Rebecq, Daniel Gehrig, and Davide Scaramuzza, "ESIM: an open event camera simulator," in *Conf. on Robotics Learning (CoRL)*, 2018. 6

[37] Bongki Son, Yunjae Suh, Sungho Kim, Heejae Jung, Jun-Seok Kim, Changwoo Shin, Keunju Park, Kyoobin Lee, Jinman Park, Jooyeon Woo, Yohan Roh, Hyunku Lee, Yibing Wang, Ilia Ovsiannikov, and Hyunsurk Ryu, "A 640x480 dynamic vision sensor with a 9um pixel and 300Meps address-event representation," in *IEEE Intl. Solid-State Circuits Conf. (ISSCC)*, 2017. 7, 8

[38] Elias Mueggler, Henri Rebecq, Guillermo Gallego, Tobi Delbruck, and Davide Scaramuzza, "The event-camera dataset and simulator: Event-based data for pose estimation, visual odometry, and SLAM," *Int. J. Robot. Research*, vol. 36, no. 2, pp. 142–149, 2017. 8

[39] Henri Rebecq, Guillermo Gallego, Elias Mueggler, and Davide Scaramuzza, "EMVS: Event-based multi-view stereo—3D reconstruction with an event camera in real-time," *Int. J. Comput. Vis.*, vol. 126, pp. 1394–1414, Dec. 2018. 8